Supporting Information

Electron-enrichment Enables RuPd toward 1.40 V Overall Water Splitting

Yuqin Yin[1,2], Hongyu Zhao[1,2],Zhanghu Yu[1,2], Guanren Ge[1,2], Shiyuan Feng [3],Haoyu Zhou[3], Kaiyang Sun[4], Jie Du[1,2], Tong Chen[1,2], Zhihao Yang[1,2], Jun Yu[1,2], Shichun Mu[1,2]**

[1]State Key Laboratory of Advanced Technology for Materials Synthesis and Processing, Wuhan University of Technology, Wuhan 430070, China

[2]Key Laboratory of Fuel Cell Technology of Hubei Province, Wuhan 430070, China

[3]School of Materials Science and Engineering, Wuhan University of Technology, Wuhan 430070, China

[4]College of Chemistry & Chemical Engineering, Northwest Normal University, Lanzhou 730000, China.

*Corresponding Authors: yujun@whut.edu.cn, msc@whut.edu.cn.

1.Experimental Details

1.1 Materials and Reagents

Nickel nitrate hexahydrate ($Ni(NO_3)_2·6H_2O$),Ferrous sulfate heptahydrate ($FeSO_4·7H_2O$),Ruthenium chloride hydrate ($RuCl_3·xH_2O$) Palladium chloride hydrate ($PdCl_3·xH_2O$)was purchased from Aladdin. Potassium hydroxide (KOH),absolute ethanol, and hydrochloric acid were purchased from Beijing Chemical Works.RuO2, Pt/C (20 wt%) powder, and Nafion solution (5 wt%) were purchased fromSigma-Aldrich. All the reagents are analytical grade and used without further treatment Natural seawater was obtained fromthe Yellow Sea of China and filtered for further use.

1.2 Synthesis of catalysts

Synthesis of RuPd-$RuNiFeO_x$/NF:1.425 g of $Ni(NO_3)_2·6H_2O$ and 0.195 g of $FeSO_4·7H_2O$ were dissolved separately in 24 mL of ethanol and 8 mL of deionized water, respectively. The two solutions were then mixed under vigorous stirring. Subsequently, 50 mg of $RuCl_3·xH_2O$ and 50 mg of $PdCl_2·xH_2O$ were added to the mixture with continued stirring. A pre-cleaned nickel foam (NF, 2 × 3 cm) was completely immersed in the resulting solution and maintained at 25 °C for 24 h. Afterwards, the NF was gently rinsed with ethanol to remove surface solvent and finally dried in a vacuum oven at 25 °C for 12 h.$NiFeO_x$/NF was synthesized according to the method described in Reference [1].1.425 g of $Ni(NO_3)_2·6H_2O$ and

0.195 g of $FeSO_4 \cdot 7H_2O$ were dissolved separately in 24 ml of ethanol and 8 ml of deionized water. The solutions were then mixed under vigorous stirring to form a solution. The pre-washed NF (2 × 3 cm) was completely immersed in the solution at 25°C for 24 hours. The same method was also used to synthesize Pd-$NiFeO_x$/NF and Ru-$NiFeO_x$/NF without adding a second metal.The preparation of $RuPdO_x$/NF: Dissolve 50 mg of RuCl3 •xH2O and 50 mg of PdCl3 •xH2O respectively in 24 mL of ethanol and 8 mL of deionized water, and then stir magnetically until completely mixed. Immerse the pre-cleaned NF (2×3 cm) completely in this solution and keep it at 25° C for 24 hours. Then wash it with deionized water and dry it in a vacuum oven at 25° C for 12 hours to obtain RuPdOx/NF.

1.3 Material Characterization

X-ray diffraction (XRD) patterns were collected on a Bruker D8-Advance X-ray diffractometer equipped with a Cu Kα radiation source. The morphology and structure were characterized by scanning electron microscopy (SEM, FEI nanoSEM450). Field emission high resolution transmission electron microscope (JEM-2100F) and double spherical aberration-corrected scanning transmission electron microscope (AC-STEM, Titan Cubed Themis G2 300). The chemical state of samples shown in XPS images was performed on an ESCALAB-250Xi spectrometer equipped with monochromatic Al Ka radiation. The Raman spectrum is tested on the Renishaw Raman Microscope (LabRAM Odyssey) to determine hydroxyl oxides. ICP-OES analysis was performed on Optima Prodigy 7.

1.4 Electrochemical Measurements

All electrochemical measurements were performed in a conventional three-electrode system at room temperature using a CHI 660E electrochemical analyzer (CHI Instruments, Shanghai, China). A graphite rod and Hg/HgO were used as the counter electrode and the reference electrode, respectively. The as-prepared electrocatalysts with a geometric area of 0.25 cm^2 were directly served as the working electrodes. As for powdery catalysts (RuO2 and Pt/C), the working electrodes were prepared by dropping electrocatalyst ink onto NF. The alkaline freshwater and seawater media were prepared by adding potassium hydroxide to freshwater and seawater (1M KOH, pH≈14), respectively. The scan rate of the polarization curves of HER and water splitting was 5mV s^{-1}, but OER was 2 mV s^{-1} in order to reduce the effect of nickel oxidation peak. In HER and OER characterizations, the polarization curves were iR-corrected using the equation: E_{iR}-corrected = E – iR, where E is the original potential, R is the solution resistance, i is the corresponding current, and EiR-corrected is the iR-corrected potential. Electrochemical impedance spectroscopy (EIS) tests were carried out in a frequency ranging from 0.01 Hz to 100 kHz with AC amplitude of 10 mV at the voltage corresponding to 300 mV overpotential (OER) and 100 mV overpotential (HER).Furthermore, the HER and OER potentials were converted to RHE scale according to the equation: E (vs. RHE) = E (vs. Hg/HgO) + 0.059*pH + 0.098 V. The electrochemical double layer capacitance (C_{dl}) was

determined with typical cyclic voltammetry (CV) measurements at various scan rates (2, 4, 6, 8 and 10 mV s^{-1}) in 0.93~ 1.03 V (for OER) and (0.05) ~ (0.15) V (for HER) versus RHE. The C_{dl} can be further converted into ECSA using the specific capacitance value for a standard with 1cm^{-2} of real surface area. The specific capacitance for a flat surface is normally between0.02-0.06 mF cm^{-2}.

1.5 **DFT calculations**

All computations were carried out using the Vienna Ab initio Simulation Package (VASP). The electron exchange-correlation potential was treated within the generalized gradient approximation (GGA) using the Perdew–Burke–Ernzerhof (PBE) functional. The ion-electron interactions were described by the projector augmented wave (PAW) method. A plane-wave basis set with a kinetic energy cutoff of 400 eV was employed. The convergence criteria for energy and force were set to 10^{-5} eV and 0.02 eV $Å^{-1}$.

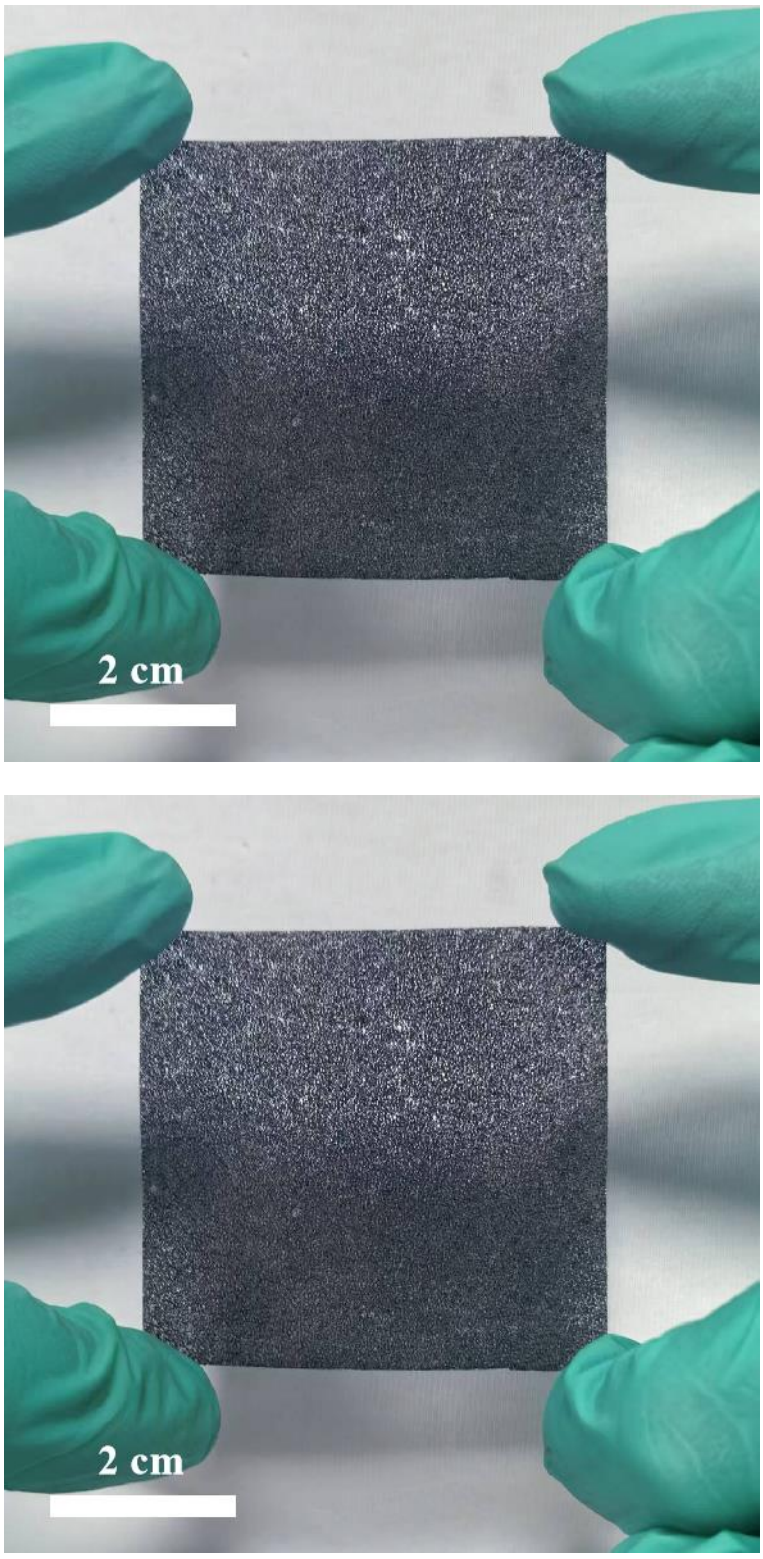

Figure S1. RuPd-RuNiFeO_x/NF catalyst generated on Ni foam.

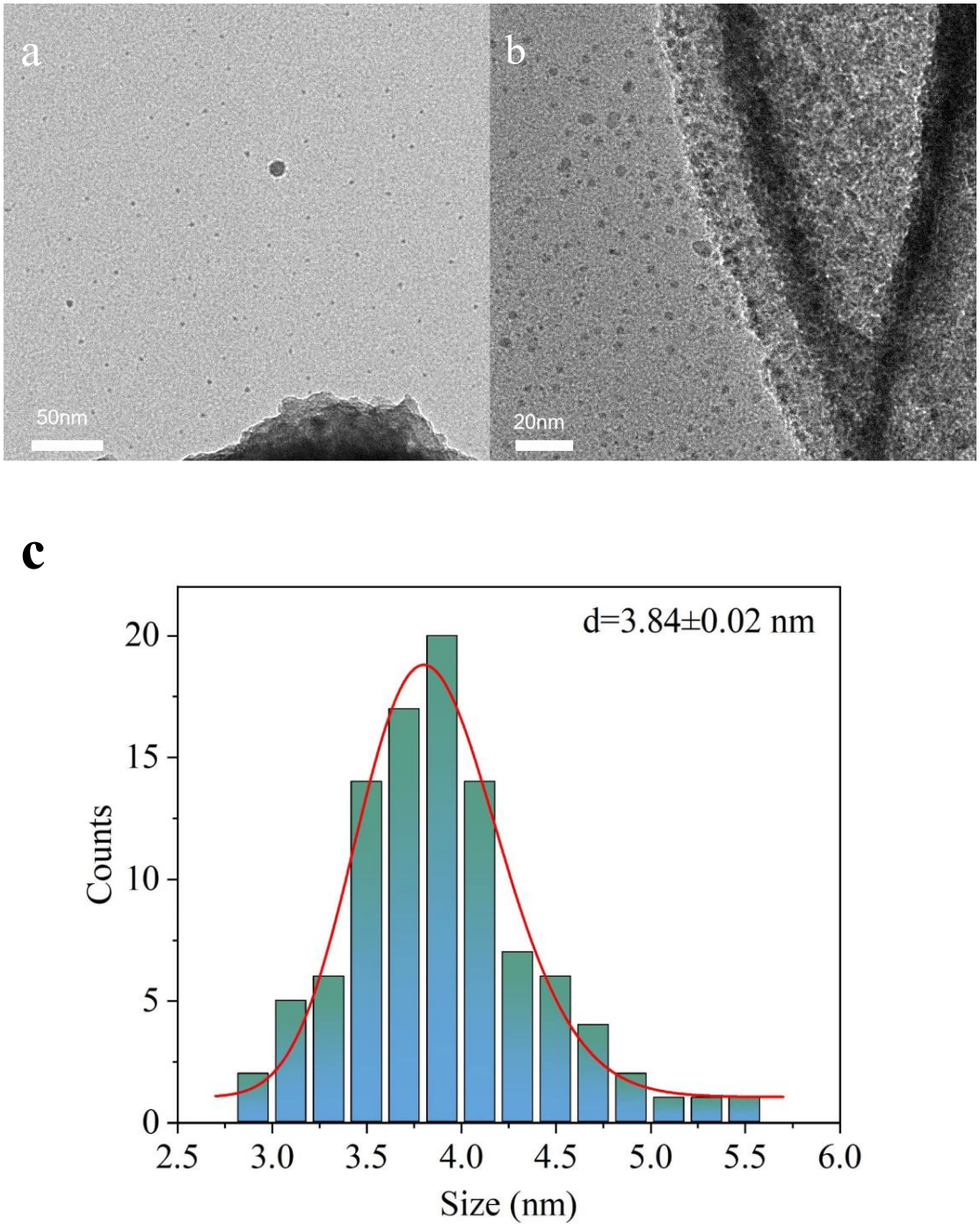

Figure S2. a,b）TEM of insoluble nanoparticles in the liquid and Statistical distribution of nanoparticles, c)The size of nanoparticles.

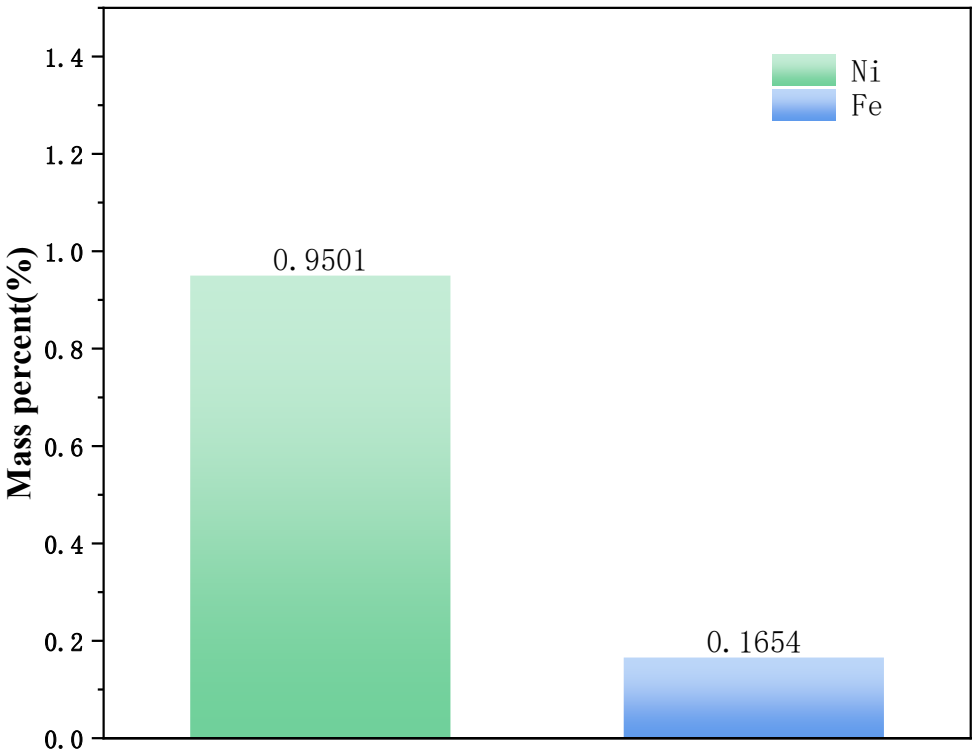

Figure S3. Ni, Fe atomic percentages in ICP-OES.

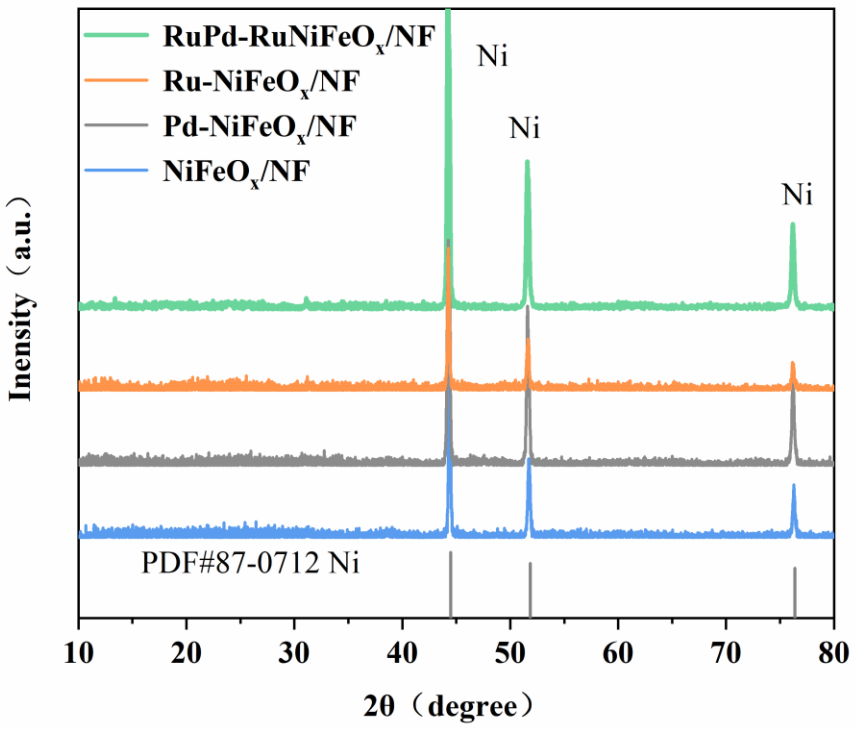

Figure S4. XRD patterns of RuPd-RuNiFeO$_x$/NF.

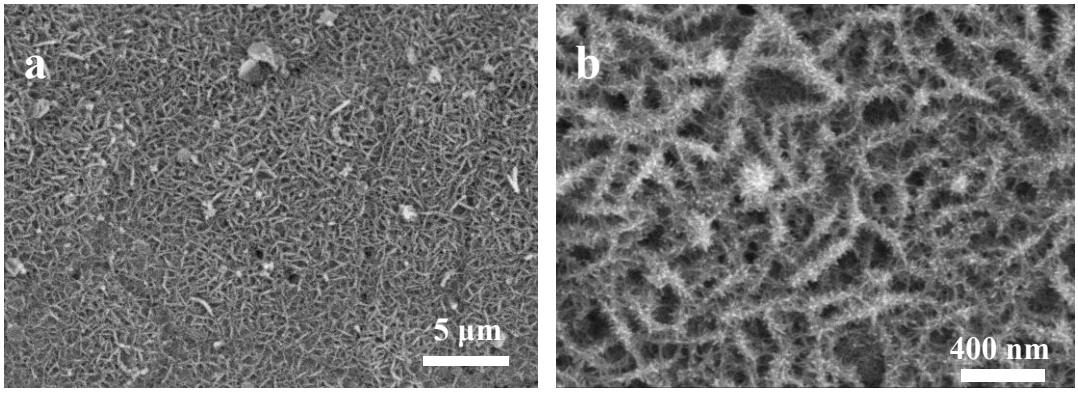

Figure S5. SEM images of $NiFeO_x$/NF a) and b).

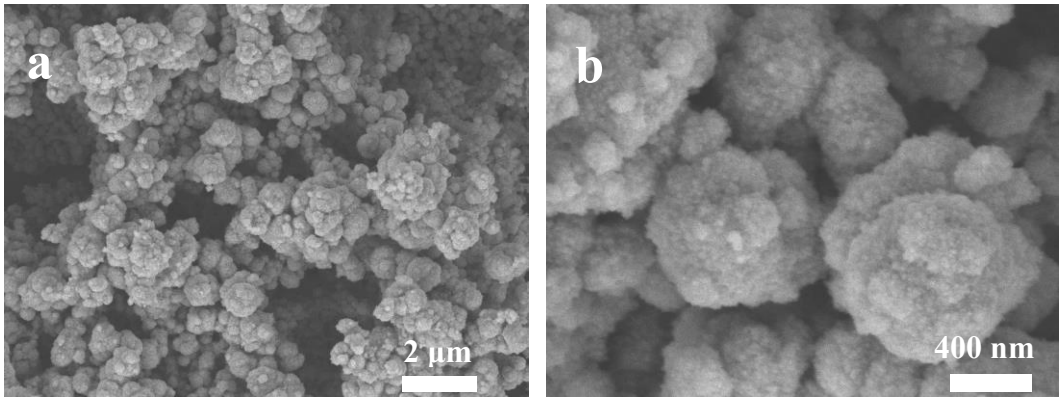

Figure S6. SEM image of RuPd-RuNiFeO_x/NF a) and b).

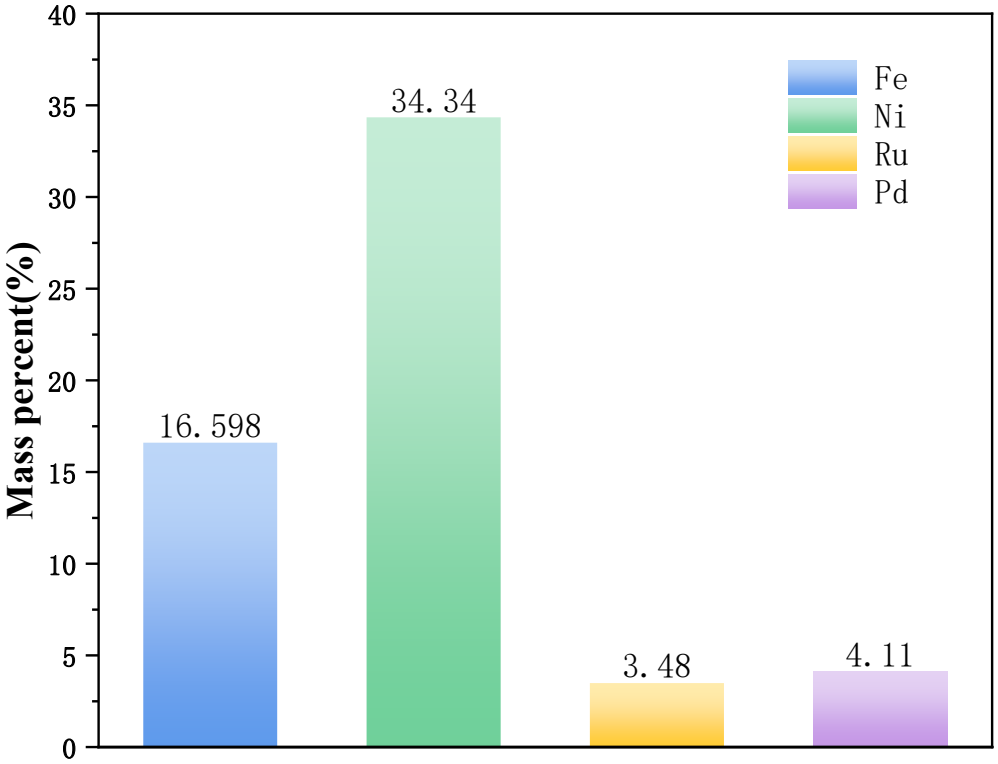

Figure S7. Ni, Fe Pd and Ru atomic percentages in ICP-OES.

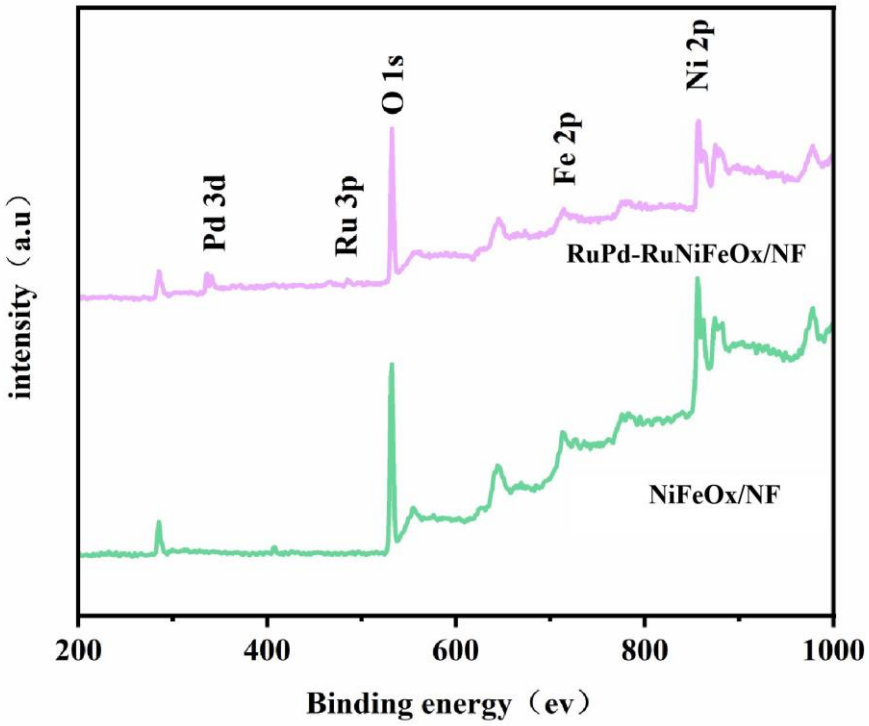

Figure S8. XPS full spectra of RuPd- RuNiFeO_x/NF and NiFeO_x/NF.

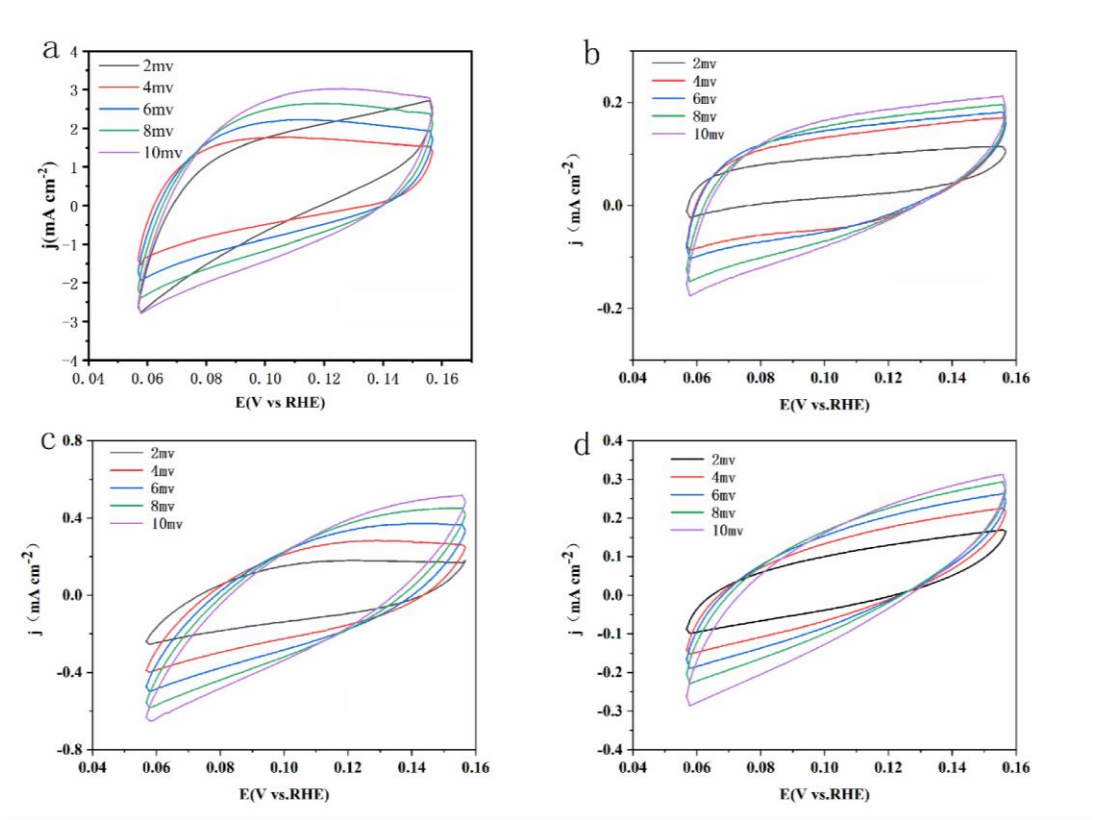

Figure S9. CV curves of a) RuPd-RuNiFeO$_x$/NF, b) Ru-NiFeO$_x$/NF, c) Pd-NiFeO$_x$/NF and d) NiFeO$_x$/NF at scan rates ranging from 2 to 10 mV s-1 outside HER region.

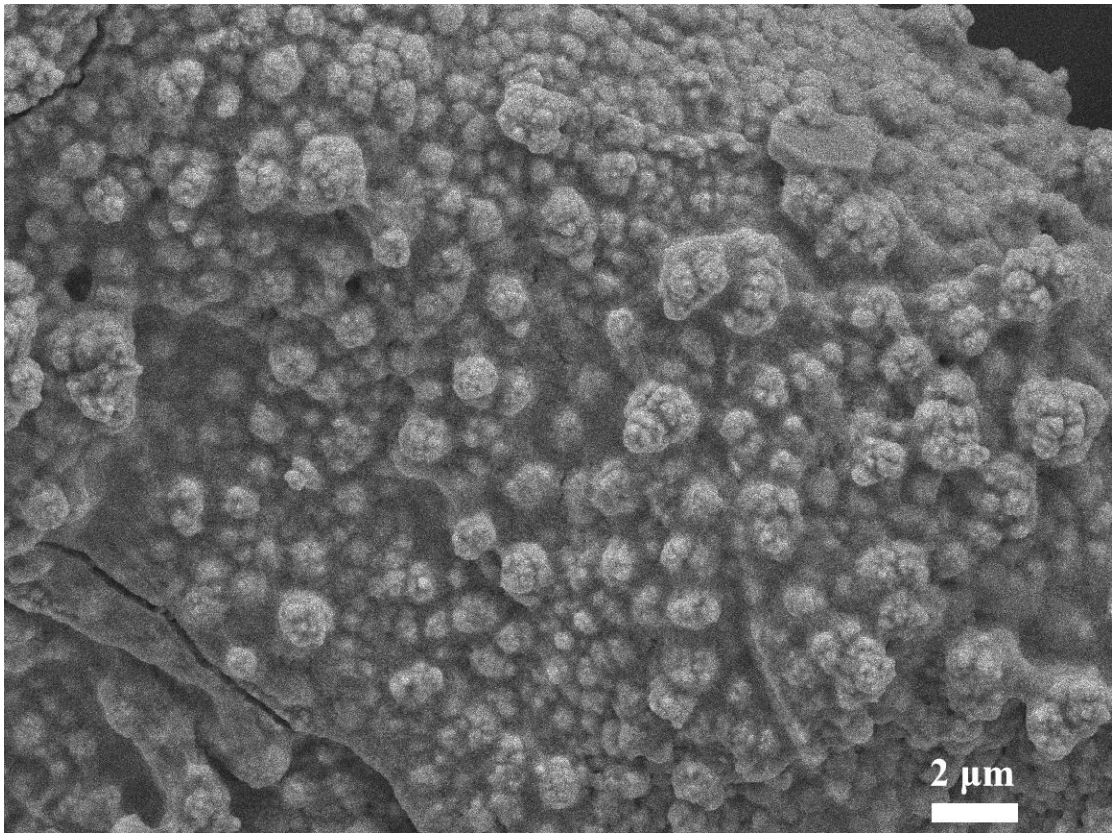

Figure S10. SEM image of RuPd- RuNiFeO_x/NF after HER.

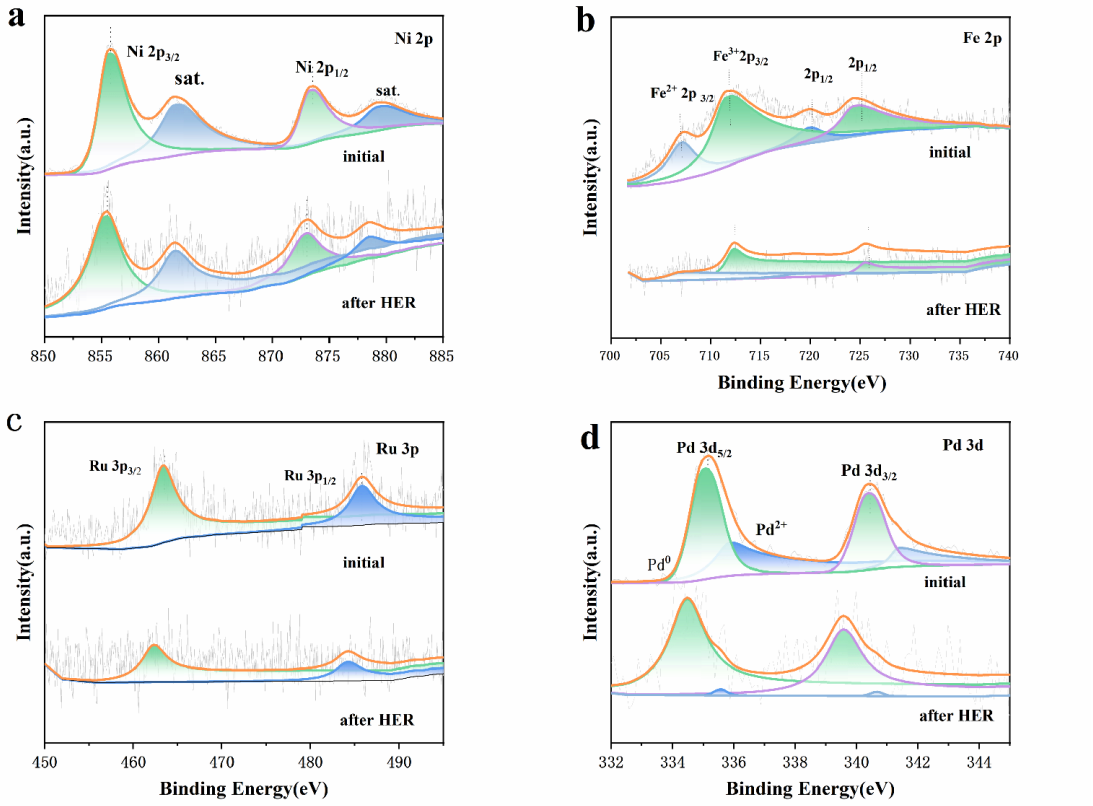

Figure S11. High resolution XPS spectra of RuPd- $RuNiFeO_x$/NF before and after HER test

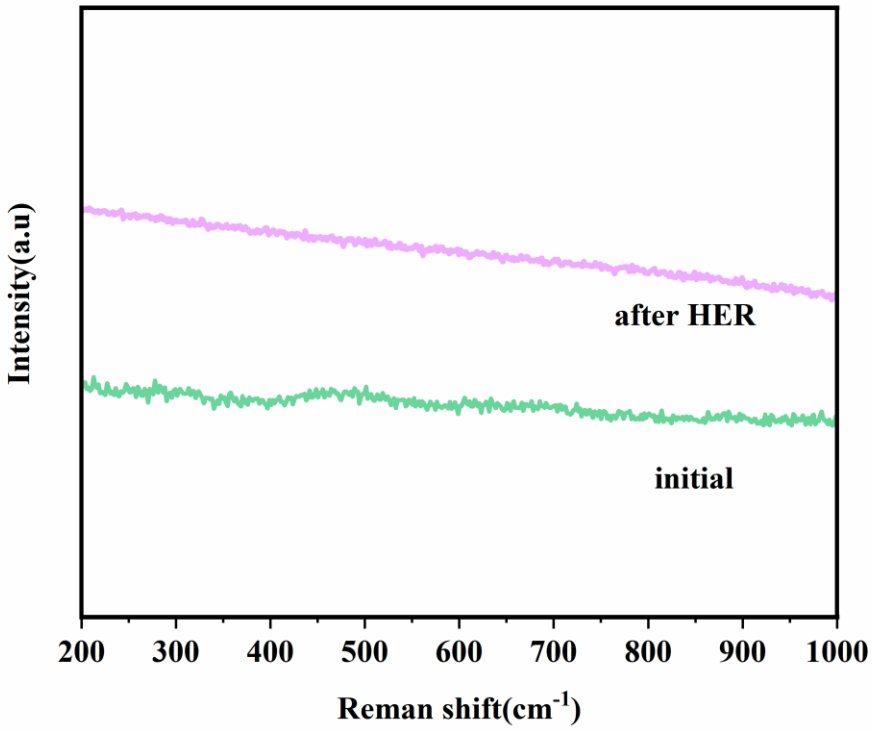

Figure S12. Raman spectra of RuPd-RuNiFeO_x /NF before and after HER test.

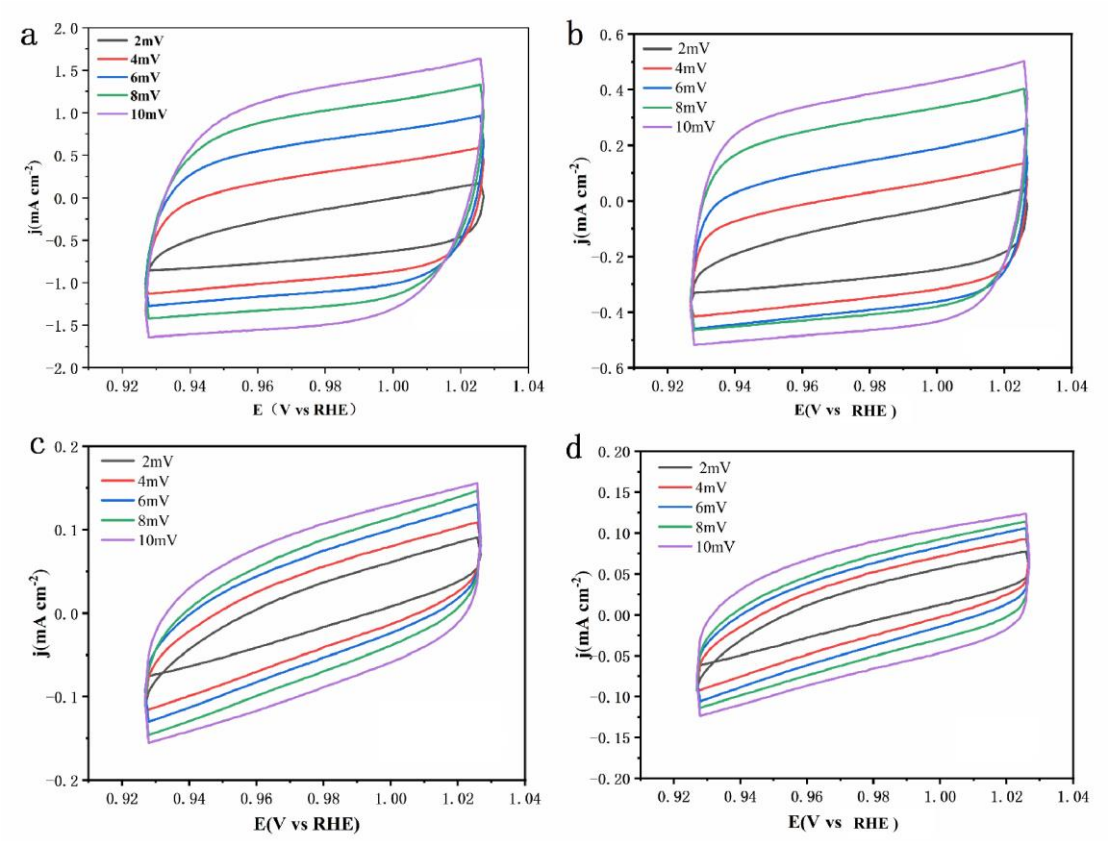

Figure S13. CV curves of a) RuPd-RNiFeO$_x$/NF, b) Ru-NiFeO$_x$/NF, c) Pd-NiFeO$_x$/NF and d) NiFeO$_x$/NF at scan rates ranging from 2 to 10 mV s-1 outside OER.

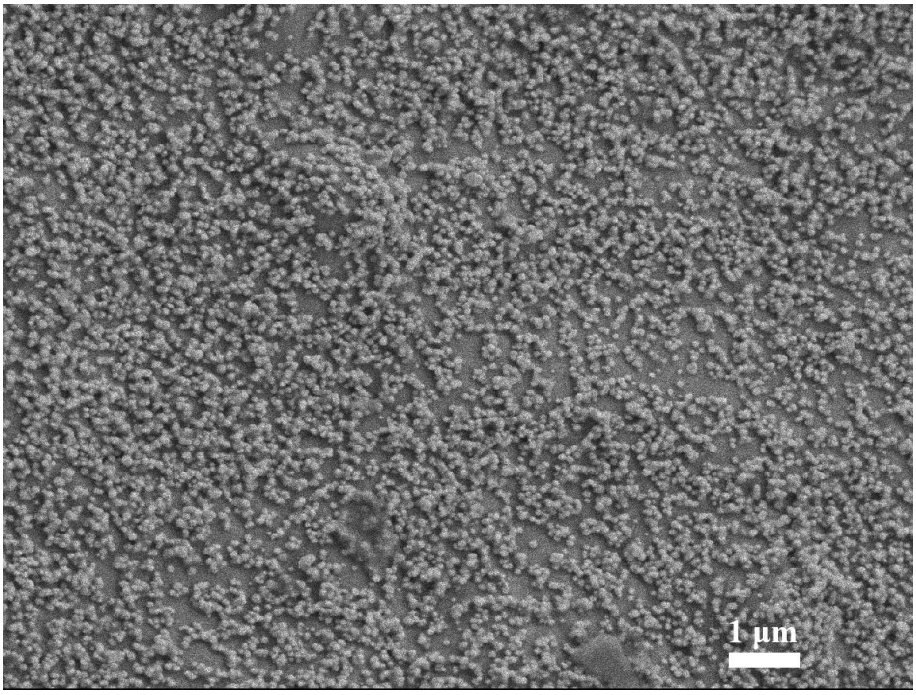

Figure S14. SEM image of RuPd-RuNiFeO_x/NF after OER test.

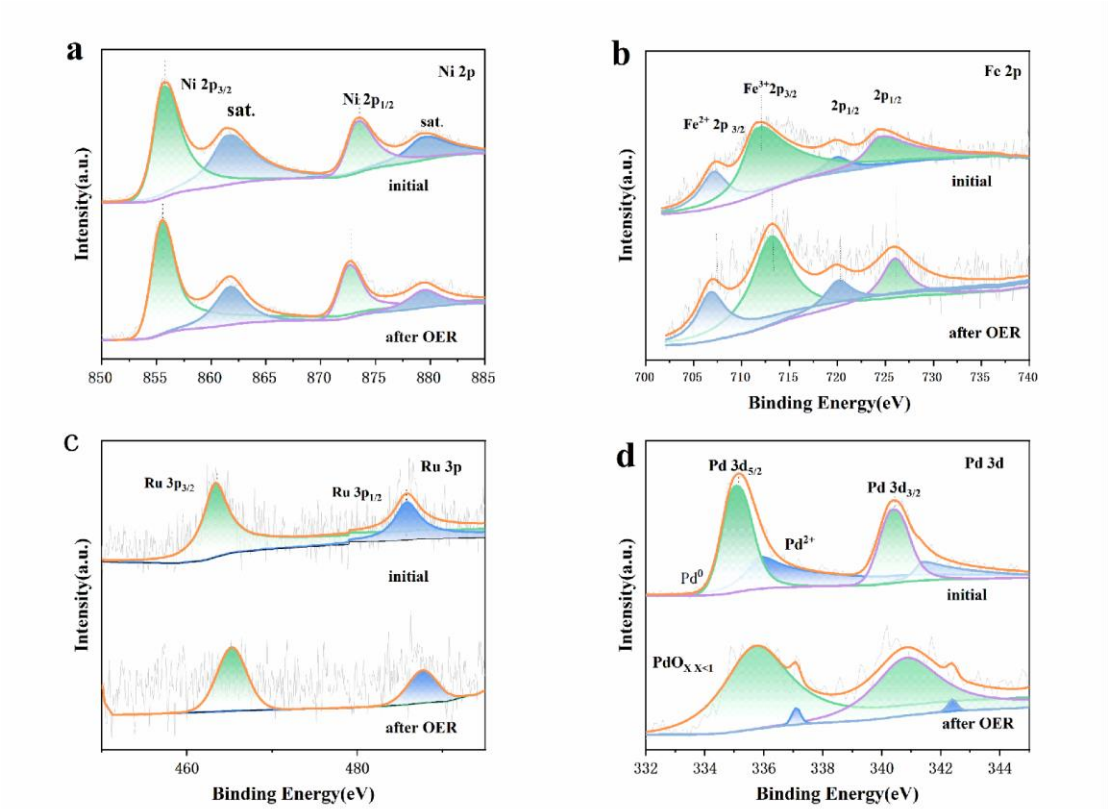

Figure S15. High resolution XPS spectra of RuPd-RuNiFeO$_x$/NF before and after OER test

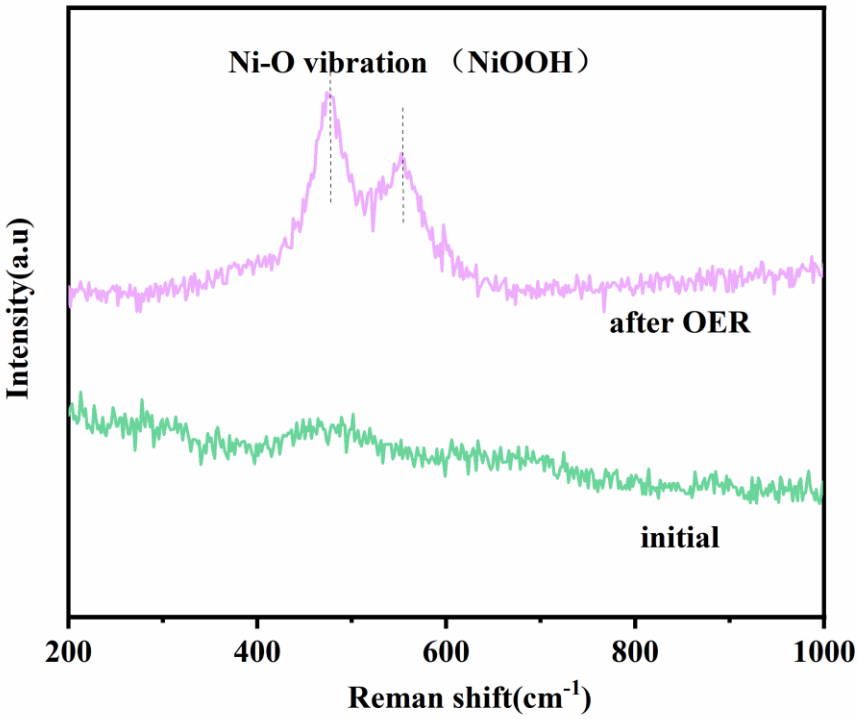

Figure S16. Raman spectra of RuPd-RuNiFeO_x/NF before and after OER test.

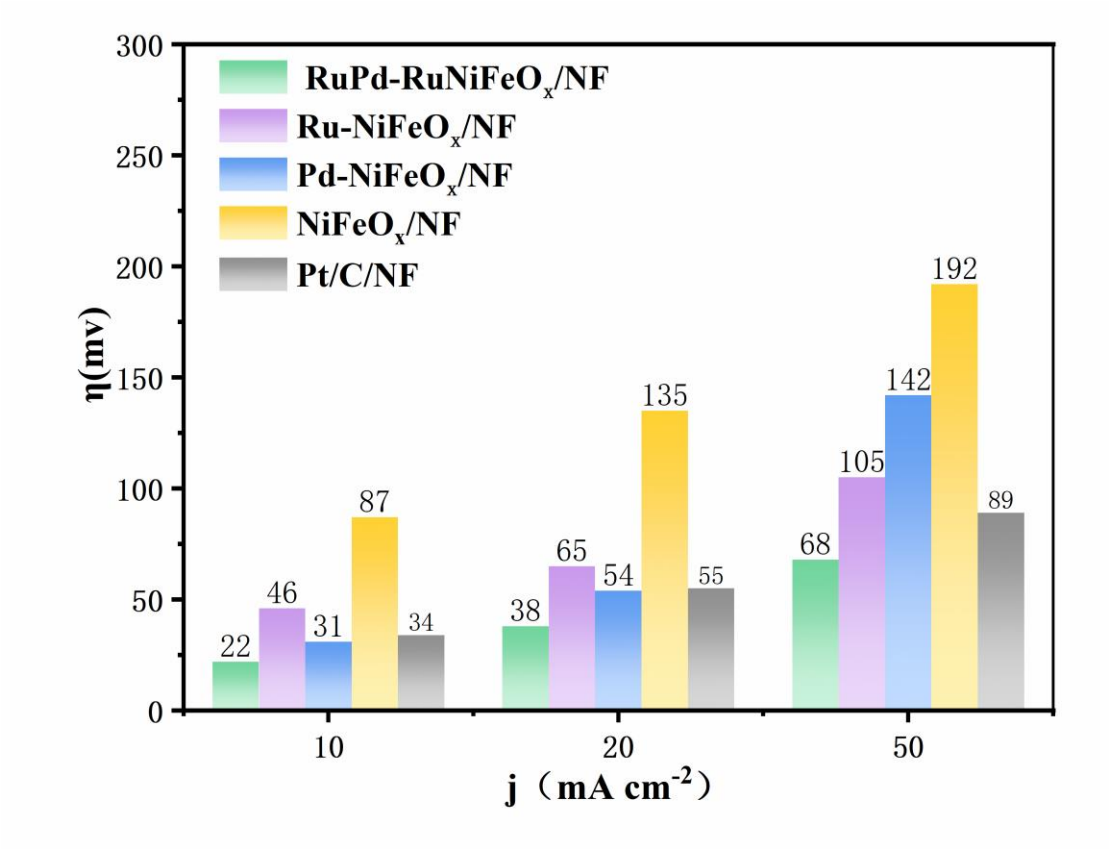

FiFigure S17. Corresponding overpotentials @10, 20,50 mA cm^{-2} during HER for RuPd-RuNiFeO$_x$ Ru-NiFeO$_x$ Pd-NiFeO$_x$, NiFeO$_x$, and commercial Pt/C tested in 1 M KOH seawater.

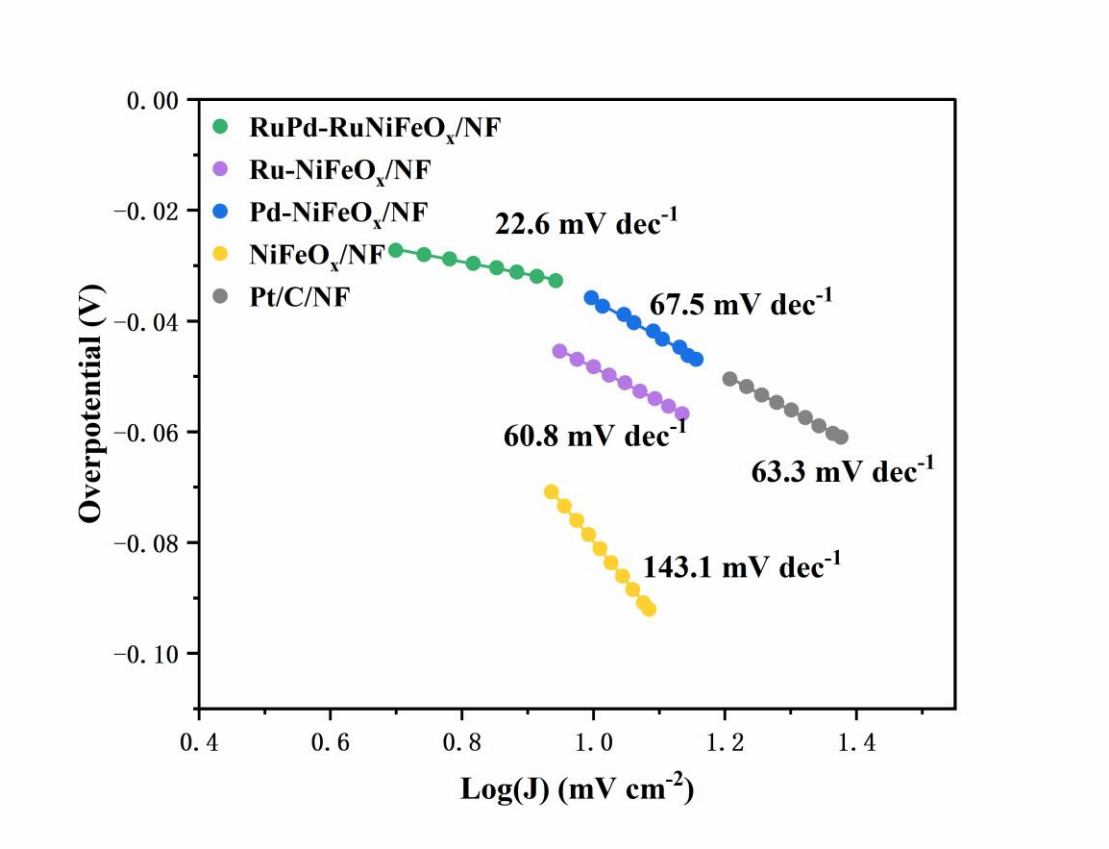

Figure S18. Tafel slopes of RuPd-RuNiFeO$_x$, Ru-NiFeO$_x$, Pd-NiFeO$_x$, NiFeO$_x$, and commercial RuO_2 tested in 1 M KOH seawate toward HER.

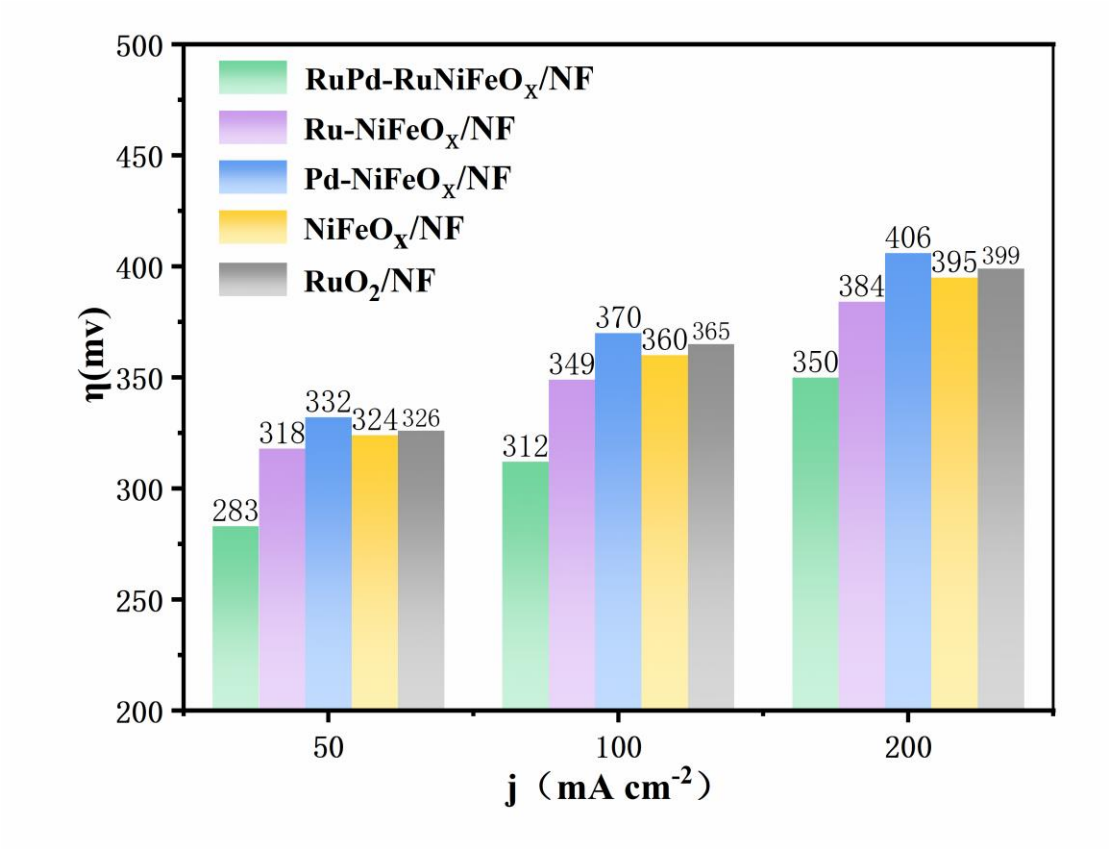

Figure S19. Corresponding overpotentials @ 50, 100, 200 mA cm^{-2} during OER for RuPd-RuNiFeO$_x$, Ru-NiFeO$_x$, Pd-NiFeO$_x$, NiFeO$_x$, and commercial RuO$_2$ tested in 1 M KOH seawater.

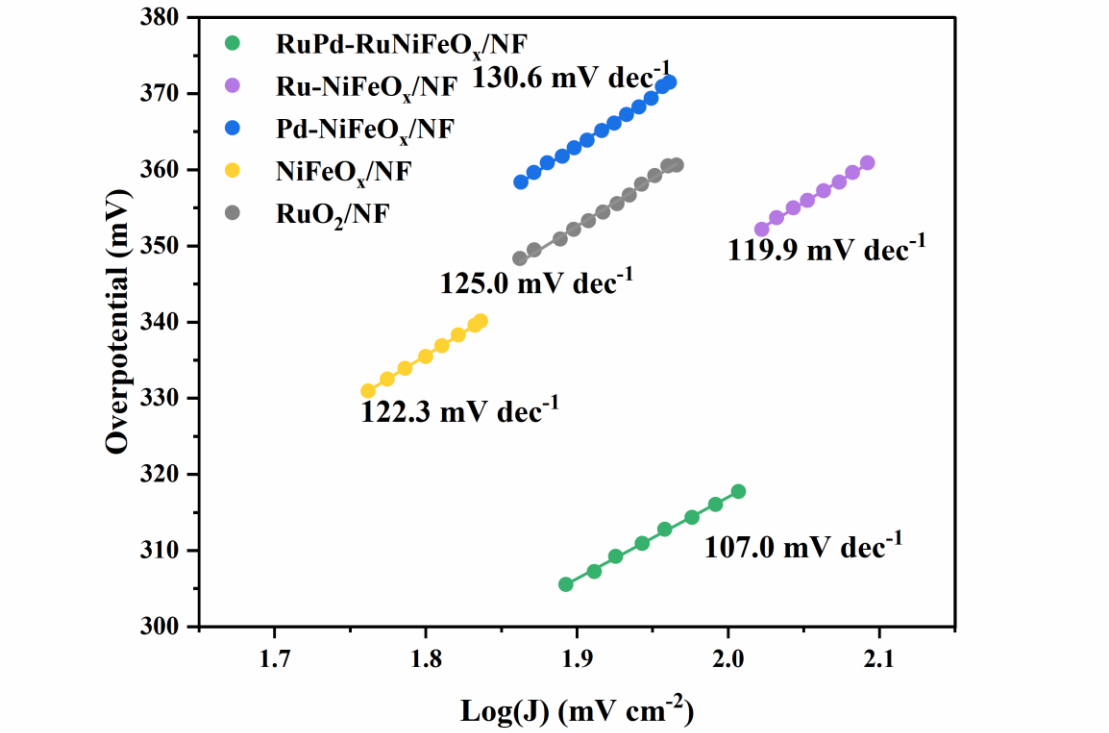

Figure S20. Tafel slopes of RuPd-RuNiFeO$_x$, Ru-NiFeO$_x$, Pd-NiFeO$_x$, NiFeO$_x$, and commercial RuO$_2$ tested in 1 M KOH seawater for OER.

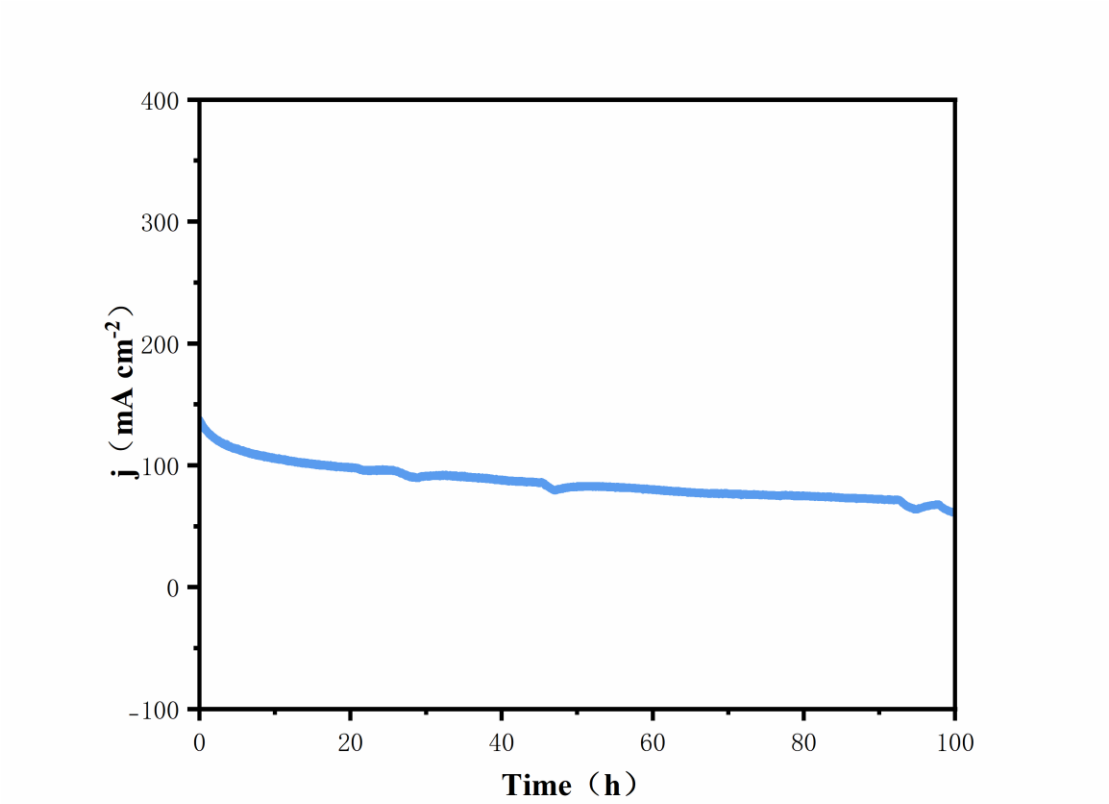

FigureS21.Chronopotentiometric curve for RuPd-RuNiFeOx/NF||RuPd-RuNiFeOx /NF for water splitting in 1 M KOH seawater.

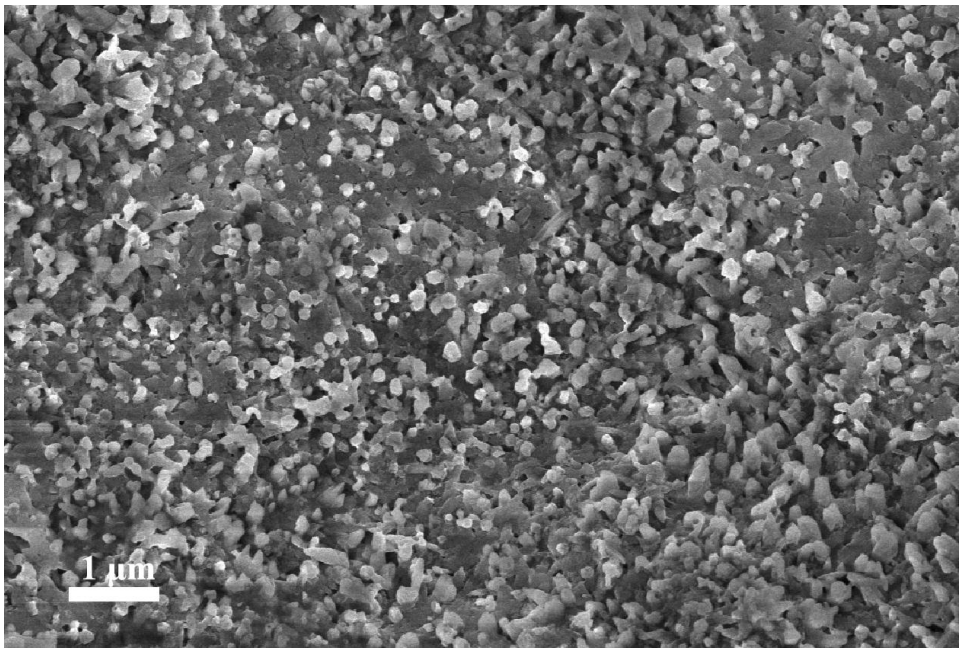

Figure S22. SEM image of RuPd-RuNiFeO_x/NF after OER test in 1 M KOH alkaline seawater electrolyte..

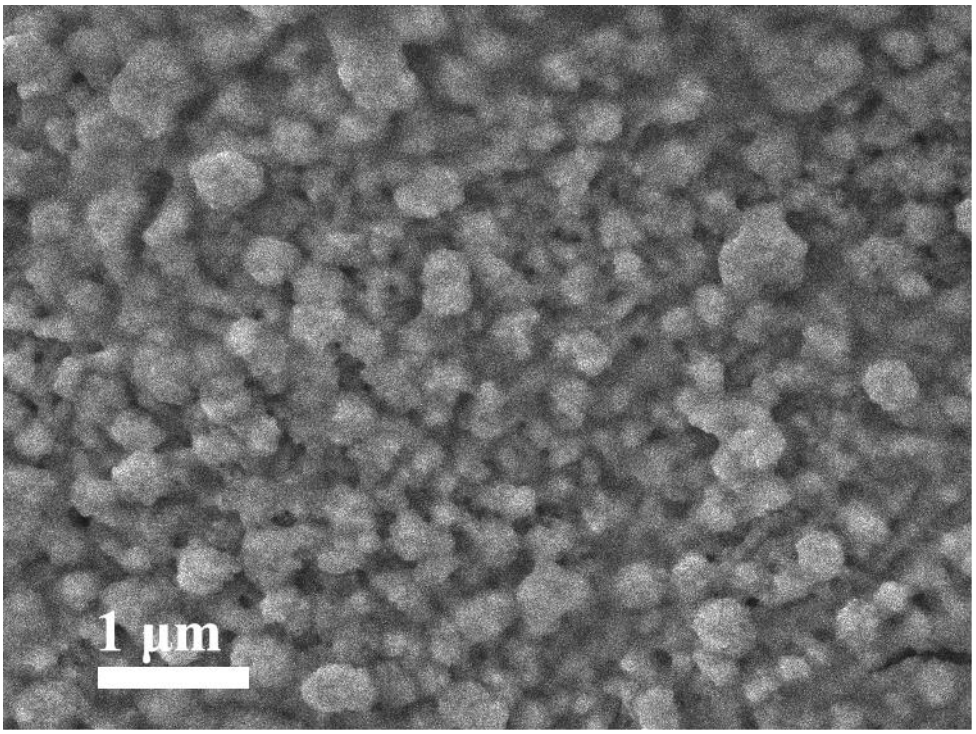

Figure S23. SEM image of RuPd-RuNiFeO_x/NF after HER test in 1 M KOH alkaline seawater electrolyte. .

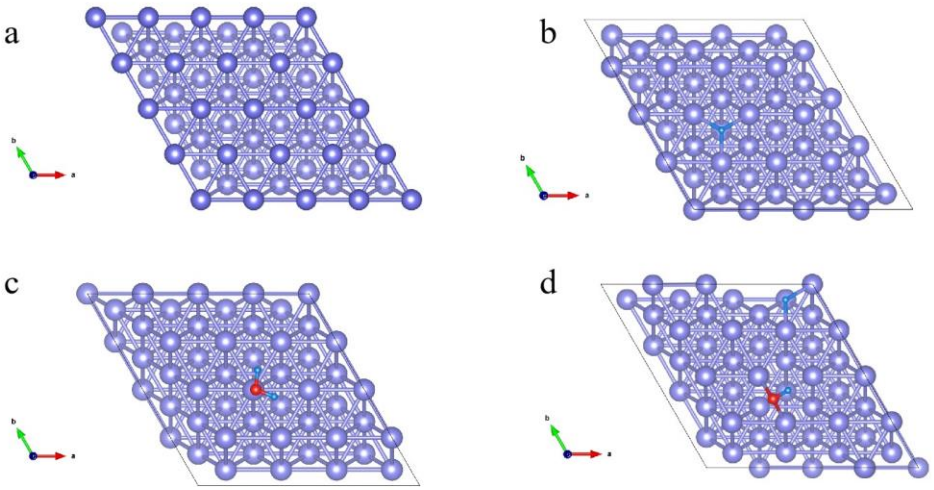

Figure S24. Theoretical structure model of Pd and Pd adsorption intermediates.

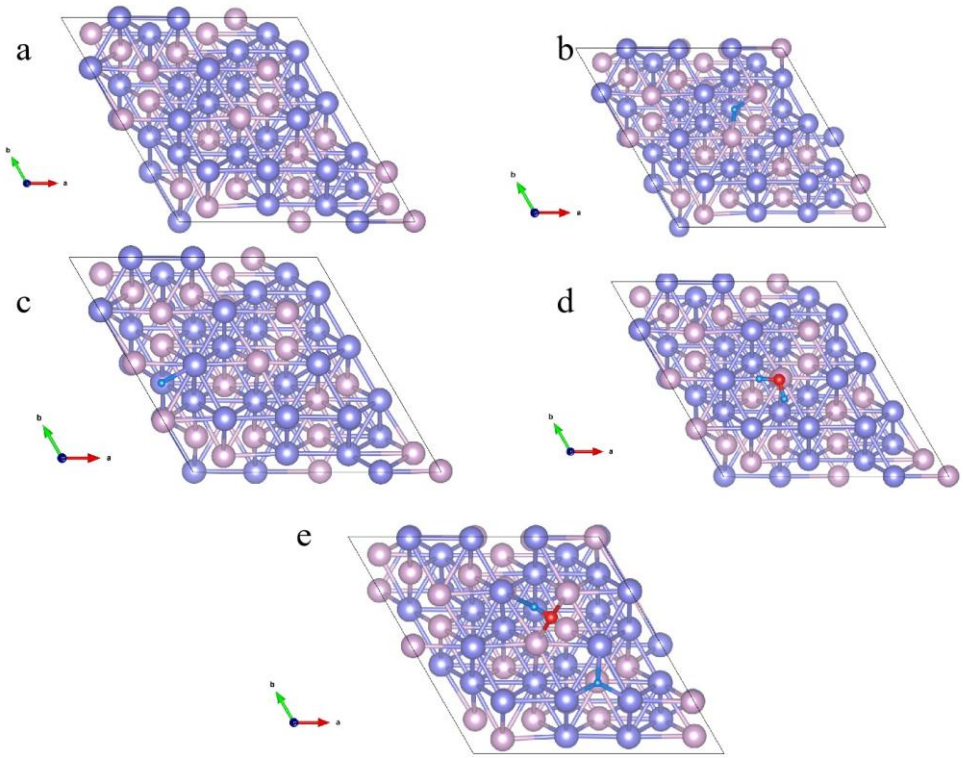

Figure S25. Theoretical structure model of RuPd and RuPd adsorption intermediates.

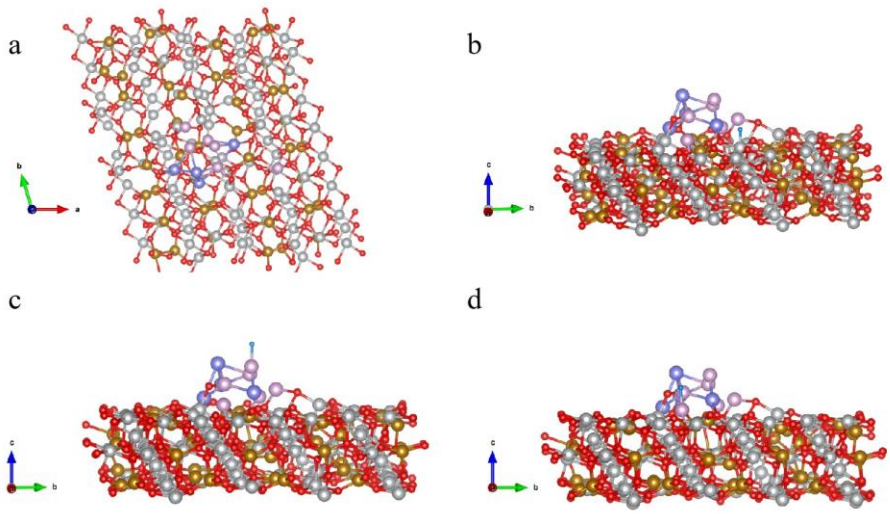

Figure S26. Theoretical structure model of RuPd-NiFeOx-Vo and RuPd-NiFeOx-Vo-H adsorption intermediates.

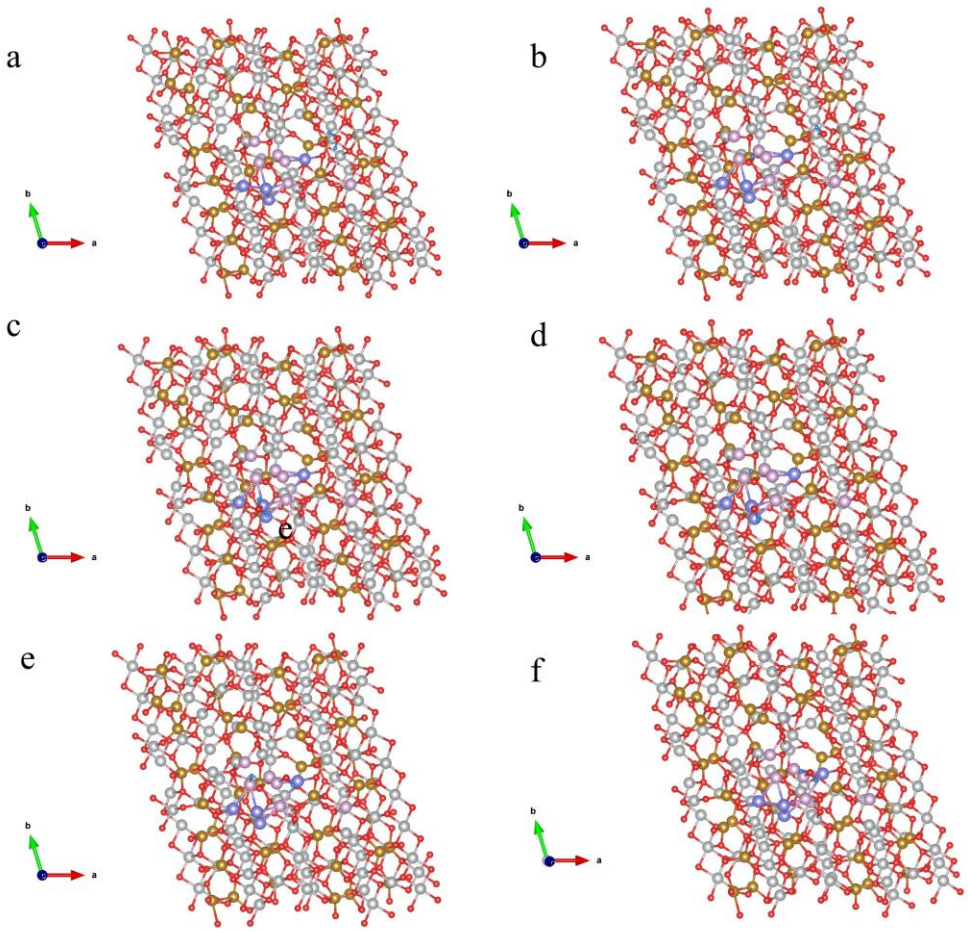

Figure S27. Theoretical structure model of RuPd-NiFeOx-Vo-H_2O and RuPd-NiFeOx-Vo-H-OH adsorption intermediat.

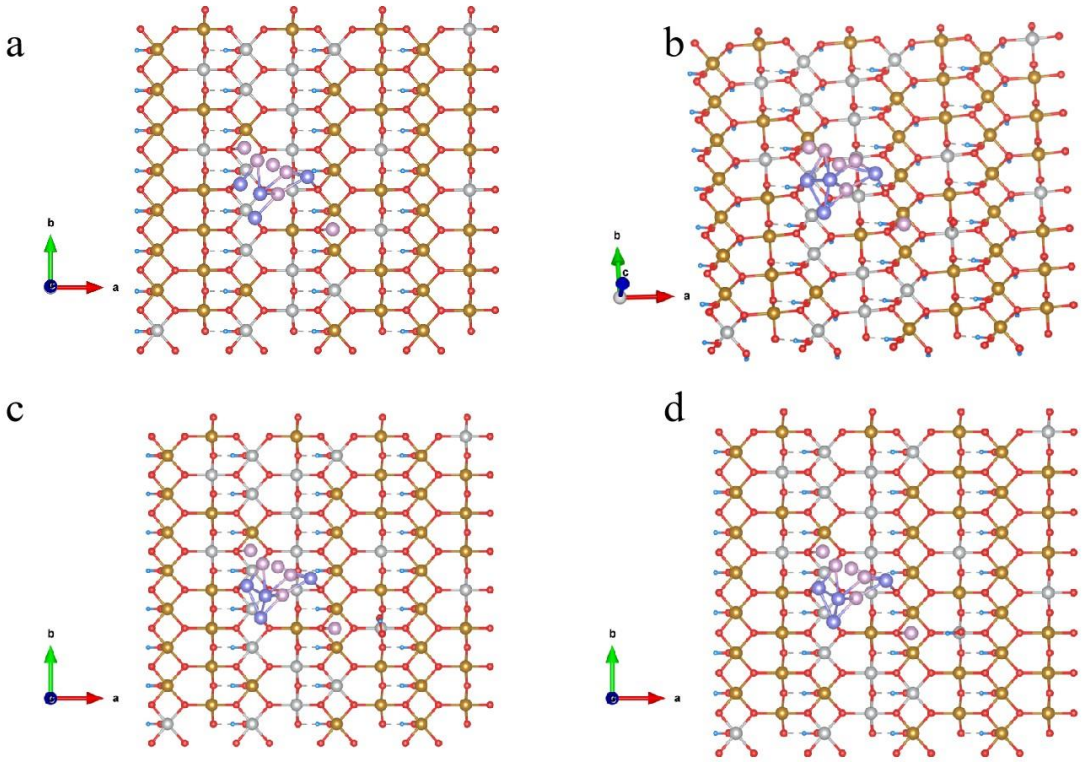

Figure S28. Theoretical structure model of RuPd-NiFeOOH and RuPd-NiFeOOH adsorption intermediates at Ni site.

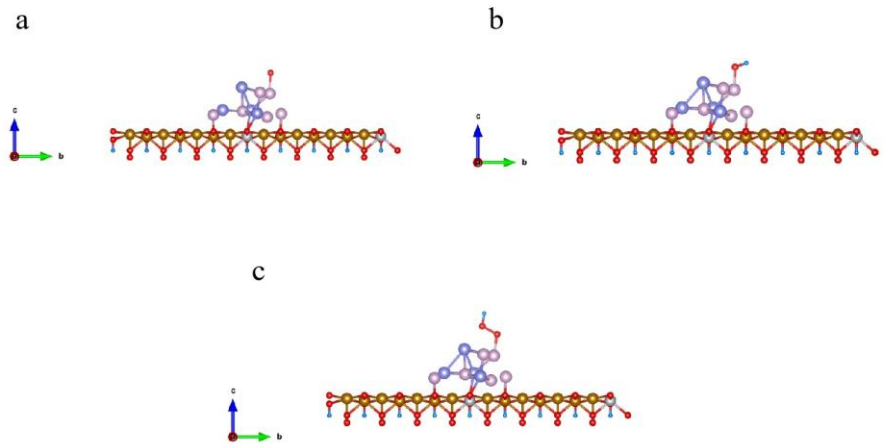

Figure S29. Theoretical structure model of RuPd-NiFeOOH and RuPd-NiFeOOH adsorption intermediates at Ru site.

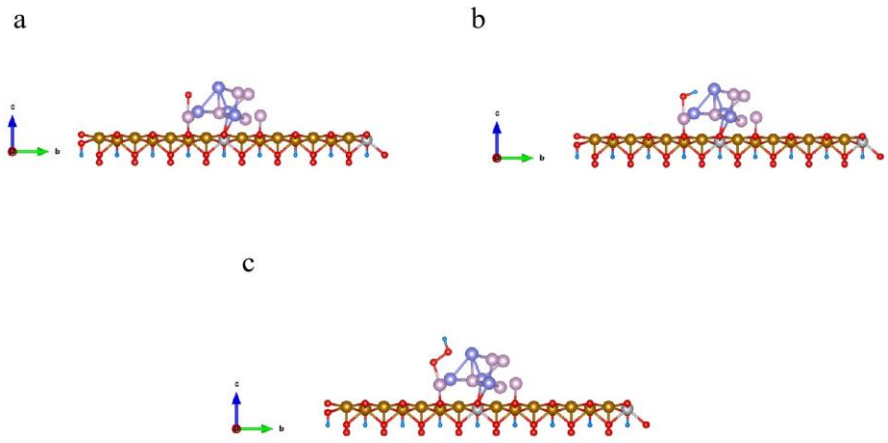

Figure S30. Theoretical structure model of RuPd-NiFeOOH and RuPd-NiFeOOH adsorption intermediates at Ru single-atom site.

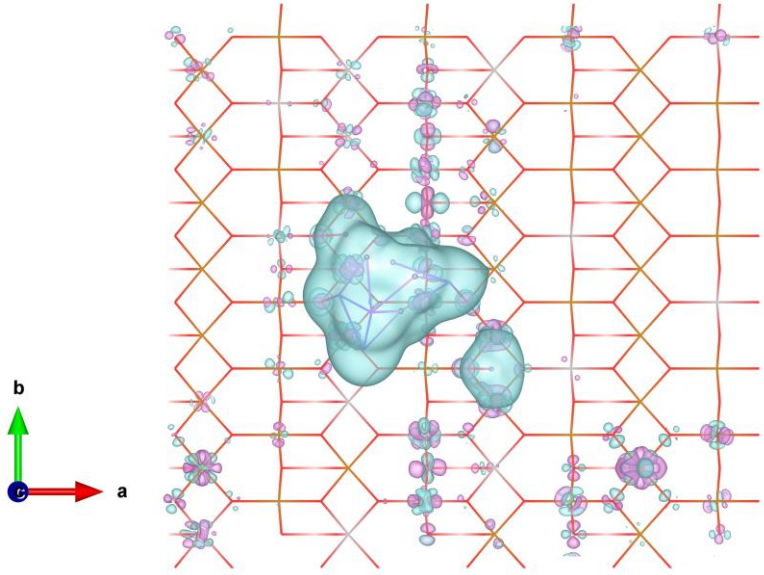

Figure S31. The DCD of RuPd-NiFeOOH.

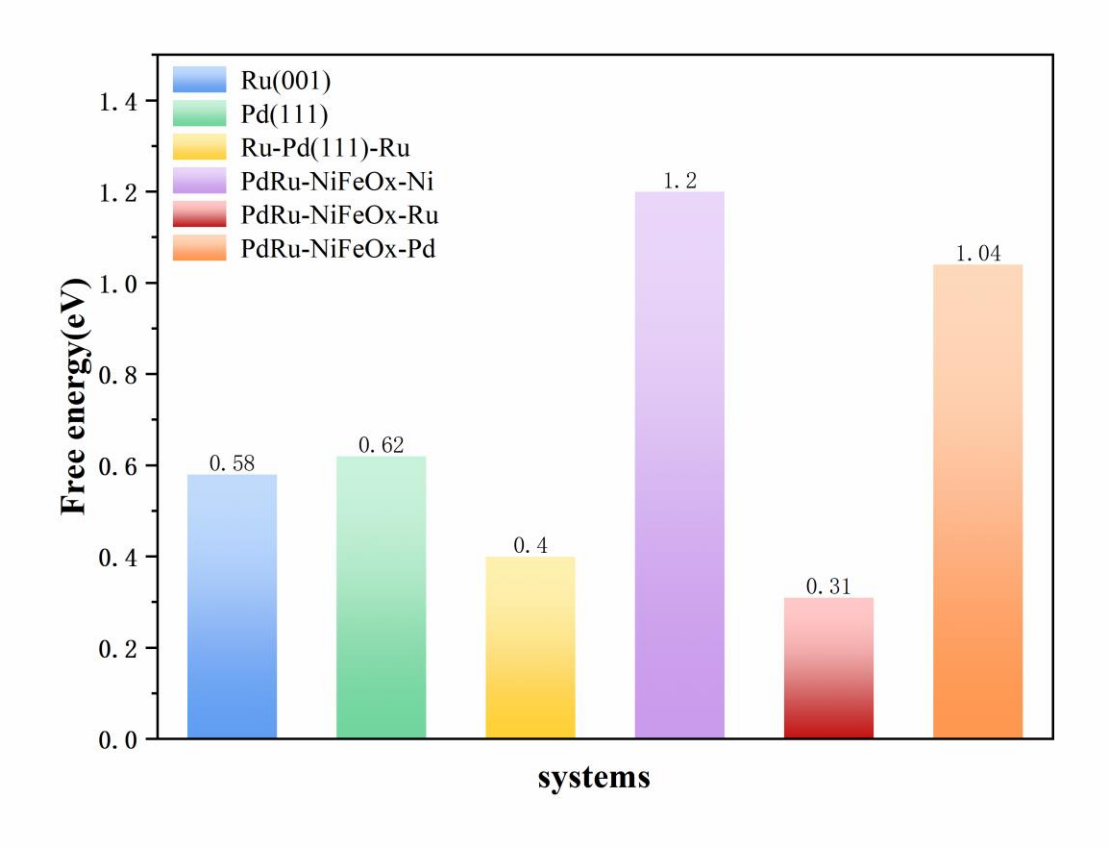

Figure S32. The dissociation free energy of different samples

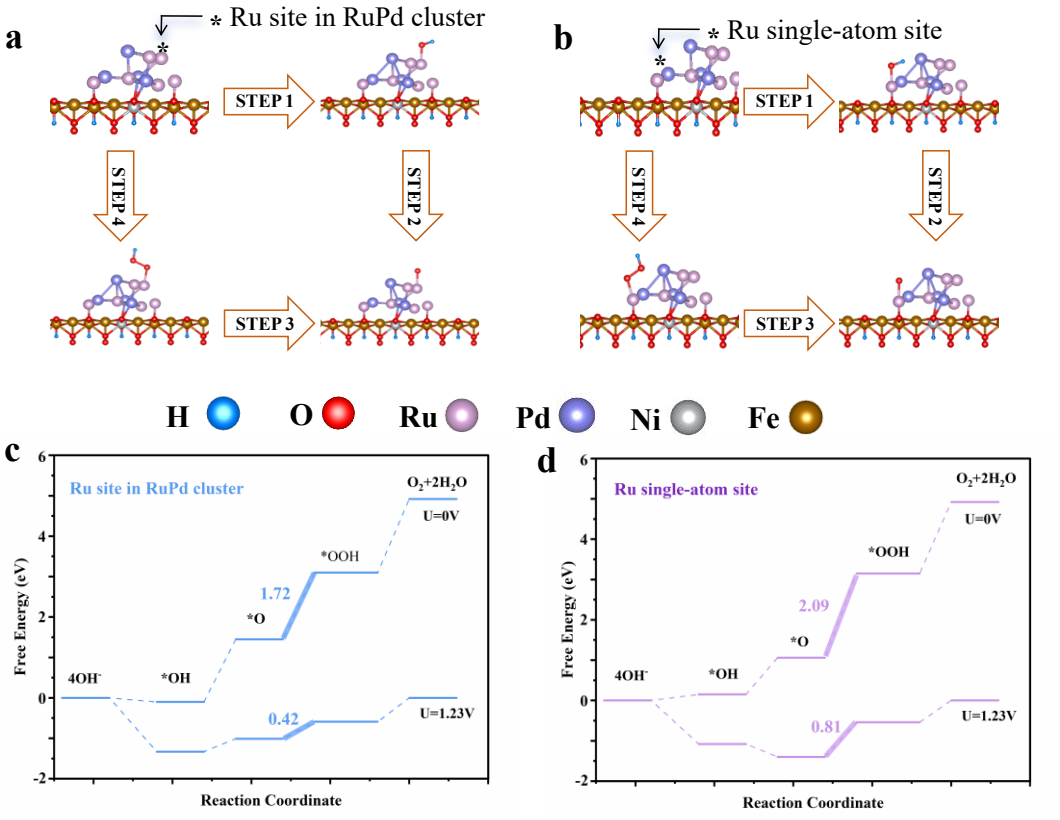

Figure S33 .Distinct roles of Ru sites in different configurations for the OER. (a) Schematic illustration of the OER pathway on the Ru site within the electron-enriched RuPd cluster. (b) Schematic illustration of the OER pathway on an Ru single-atom (Ru_{sa}) site. (c, d) Corresponding Gibbs free energy diagrams for the OER at the Ru site (in cluster) and the Ru_{sa} site.

Table S1. Ni, Fe, Pd, Ru, Pd, C and O atomic percentages of RuPd- $RuNiFeO_x$/NF in XPS survey scan.

Element	**Ni**	**Fe**	**Pd**	**Ru**	**C**	**O**
Atomic ratio	9.87	2.18	1.45	0.29	28.77	57.44

Table S2. Comparison of HER performance of RuPd-RuNiFeOx/NF with other reported highly active HER electrocatalysts in 1 M KOH freshwater.

Catalysts	**Overpotential (mV) at 10 mA cm^{-2}**	**Reference**
RuPd-RuNiFeOx/NF	17	This work
Ru-CoMoO4–x/NF	20	[2]
Ru–MnFeP/NF	35	[3]
Ni-Ru@Fe/C@CNT	32	[4]
Ru–MoO_x/NF	12	[5]
Ru-NiMoO(P)4	26	[6]
PdOx/AgMnO_4	58	[7]
RuO_2/Co_3O_4	89	[8]
Ru_1/D-NiFe LDH	18	[9]
CoNiRu-NT	22	[10]
$Ir_{44}Pd_{56}$/KB	18	[11]
AC-HEA-CuAgAuPtPd	20	[12]

Table S3. The value of C_{dl} and corresponding ECSA for RuPd- $RuNiFeO_x$/NF, Ru-$NiFeO_x$/NF Pd-$NiFeO_x$/NF and $NiFeO_x$/NF in the region of 0.05 - 0.15.

Catalysts	**Support**	**C_{dl} (mF cm^{-1})**	**ECSA (cm^2)**
RuPd- $RuNiFeO_x$	NF	235.5	117.75
Ru-$NiFeO_x$	NF	33.6	16.8
Pd-$NiFeO_x$	NF	17.95	8.98
$NiFeO_x$	NF	17.73	8.86

Table S4. Comparison of OER performance of RuPd-RuNiFeOx/NF with other reported highly active OER electrocatalysts in 1 M KOH freshwater.

Catalysts	**Overpotential@j(mV@mAcm-2)**	**Reference**
RuPd-RuNiFeOx/NF	263@50	This work
Ru–MnFeP/NF	270@100	[3]
Ni-Ru@Fe/C@CNT	246@10	[4]
Ru-NiMoO(P)4	265@100	[6]
Ru_1/D-NiFe LDH	218@100	[9]
CoNiRu-NT	335@100	[10]
$Ir_{44}Pd_{56}$/KB	385@100	[11]
Ru-CoP/NC	330@10	[13]
Ru-NiCo	291@100	[14]
$CoFeO_x$@BP	248@10	[15]

Table S5. The value of C_{dl} and corresponding ECSA for RuPd-$RuNiFeO_x$/NF, Ru-$NiFeO_x$/NF, Pd-$NiFeO_x$/NF and $NiFeO_x$/NF in the region of 0.93-1.03.

Catalysts	**Support**	**C_{dl}（mF cm^{-1}）**	**ECSA(cm^2)**
RuPd-$RuNiFeO_x$	NF	274.92	137.46
Ru-$NiFeO_x$	NF	64.98	32.49
Pd-$NiFeO_x$	NF	17.36	8.68
$NiFeO_x$	NF	13.41	6.7

Table S6. Comparison of water splitting performance of RuPd-RuNiFeOx/NF with other reported highly active bifunctional electrocatalysts in 1 M KOH freshwater.

Catalysts	**Overpotential@j (mV@mAcm-2)**	**Reference**
RuPd-RuNiFeO_x/NF||RuPd-RuNiFeO_x/NF	1.406@10	This work
Ru–MnFeP/NF || Ru–MnFeP/NF	1.63@100	[3]
Ni-Ru@Fe/C@CNT||Ni-Ru@Fe/C@CNT	1.78@100	[4]
Ru-NiMoO(P)4||Ru-NiMoO(P)4	1.46@10	[6]
PdOx/AgMnO_4||PdOx/AgMnO	1.49@10	[7]
RuO_2/Co_3O_4||RuO_2/Co_3O_4	1.645@10	[8]
Ru_1/D-NiFe LDH||Ru_1/D-NiFe LDH	1.44@10	[9]
$Ir_{44}Pd_{56}$/KB||$Ir_{44}Pd_{56}$/KB	1.61@50	[11]
RuP/NPC||RuP/NPC	1.81@100	[16]
Co_3O_4@Mo-Co_3S_4-Ni_3S_2||Co_3O_4@Mo-Co_3S_4-Ni_3S_2	1.62@10	[17]

References

1 Z. Li, G. Lin, L. Wang, H. Lee, J. Du, T. Tang, G. Ding, R. Ren, W. Li, X. Cao, S. Ding, W. Ye, W. Yang and L. Sun, *Nat. Catal.*, 2024, **7**, 944–952.

2 J. Wang, X. Zhao, Y. Zhang, Y. Dong, Y. Yin, Z. Yu, G. Ge, J. Yu and S. Mu, *ACS Appl. Nano Mater.*, 2025, **8**, 631–638.

3 D. Chen, Z. Pu, R. Lu, P. Ji, P. Wang, J. Zhu, C. Lin, H.-W. Li, X. Zhou, Z. Hu, F. Xia, J. Wu and S. Mu, *Adv. Energy Mater*, 2020, **10**, 2000814.

4 T. Gao, X. Li, X. Chen, C. Zhou, Q. Yue, H. Yuan and D. Xiao, *Che. Eng. J.*, 2021, **424**, 130416.

5 J. Cen, E. Jiang, Y. Zhu, Z. Chen, P. Tsiakaras and P. K. Shen, *Renew Energy*, 2021, **177**, 1346–1355.

6 S. Wu, D. Chen, S. Li, Y. Zeng, T. Wang, J. Zhang, J. Yu, S. Mu and H. Tang, *Adv. Sci.*, 2023, **10**, 2304179.

7 P. Mondal, J. Satra, D. N. Srivastava, G. R. Bhadu and B. Adhikary, *ACS Catal.*, 2021, **11**, 3687–3703.

8 H. Liu, G. Xia, R. Zhang, P. Jiang, J. Chen and Q. Chen, *RSC Adv.*, 2017, **7**, 3686–3694.

9 P. Zhai, M. Xia, Y. Wu, G. Zhang, J. Gao, B. Zhang, S. Cao, Y. Zhang, Z. Li, Z. Fan, C. Wang, X. Zhang, J. T. Miller, L. Sun and J. Hou, *Nat. Commun.*, 2021, **12**, 4587.

10 Y. Wang, S. Wang, Z. Ma, L. Yan, X. Zhao, Y. Xue, J. Huo, X. Yuan, S. Li and Q. Zhai, *Adv. Mater.*, 2022, **34**, 2107488.

11 X. Yang, Z. Wu, Z. Xing, C. Yang, W. Wang, R. Yan, C. Cheng, T. Ma, Z. Zeng, S. Li and C. Zhao, *Small*, 2023, **19**, 2208261.

12 X. Yu, X. Gong, H. Qiao, X. Liu, C. Ma, R. Xiao, R. Li and T. Zhang, *Small Methods*, **n/a**, 2400793.

13 Y.-R. Hao, H. Xue, J. Sun, N. Guo, T. Song, J. Sun and Q. Wang, *ACS Appl. Mater. Interfaces*, 2021, **13**, 56035–56044.

14 J. Zhang, J. Lian, Q. Jiang and G. Wang, *Chem. Eng. J.*, 2022, **439**, 135634.

15 X. Li, L. Xiao, L. Zhou, Q. Xu, J. Weng, J. Xu and B. Liu, *Angew. Chem. Int. Ed*, 2020, **59**, 21106–21113.

16 Q. Qin, H. Jang, L. Chen, G. Nam, X. Liu and J. Cho, *Adv. Energy Mater.*, 2018, **8**, 1801478.

17 Q. Wu, A. Dong, C. Yang, L. Ye, L. Zhao and Q. Jiang, *Chem. Eng. J.*, 2021, **413**, 127482.